Heat transfer and entropy generation of turbulent forced convection flow of nanofluids in a heated pipe

Goutam Saha and Manosh C. Paul*

Systems, Power and Energy Research Division, School of Engineering, University of Glasgow, Glasgow G12 8QQ, UK
**Corresponding author*. Tel.: +44(0)141 330 8466; fax: +44(0)141 330 4343.
Email address: Manosh.Paul@glasgow.ac.uk (M.C. Paul)

Abstract:

Eulerian-Eulerian multi-phase mixture model is applied to numerically analyse the turbulent flow and heat transfer behaviours of water based Al_2O_3 and TiO_2 nanofluids in a pipe. The main goal of the present work is to investigate the effects of volume concentrations, Brownian motion and size diameter of nanoparticles on the flow and heat transfer. Analysis of entropy generation is presented in order to investigate the condition that optimises the thermal system. Results reveal that small diameter of nanoparticles with their Brownian motion has highest heat transfer rate as well as thermal performance factor for χ = 6%. Above all, the higher heat transfer rate is found while using the multi-phase model than the single-phase model (Saha and Paul [1]). Also, the optimal Reynolds number is found to be $Re = 60 \times 10^3$ for $\chi = 6\%$ and d_p = 10 *nm*, which minimises the total entropy generation. Finally, it is showed that TiO_2-water nanofluid is the most energy efficient coolant than Al_2O_3-water nanofluid, and some new correlations have been proposed for the calculation of average Nusselt number.

Key words: Nanofluid, Brownian motion, heat transfer rate, thermal performance factor, multi-phase model.

1. Introduction

Forced convection heat transfer is an important phenomenon in many engineering applications e.g. cooling of electronic components, nuclear energy, solar energy, transportation, building heating, lubrication technologies and so on. However, low thermal conductivity of conventional fluids such as water, air, engine oil and ethylene glycol is the primary limitation on the enhancement of heat transfer performance in such engineering applications. In order to achieve a better performance on the heat transfer, highly conductive nano particles are suspended in base fluid to form a nanofluid and various applications of nanofluids are highlighted in Saha and Paul [1]. Nanofluid becomes a promising alternative approach for engineering and thermal applications and research is underway to apply nanofluids in applications where the conventional heat transfer fluids are not capable of improving the desired heat transfer rate. Relevant research that covers the area of applications of turbulent nanofluid flows and heat transfer in circular pipes with single–phase assumption has been discussed in Saha and Paul [1]. We therefore particularly focus our attention here to the experimental and numerical studies which have been conducted in turbulent nanofluid flow with multi-phase approach.

For the first time, Behzadmehr *et al.* [2] numerically examined the turbulent forced convection heat transfer in a circular tube using Cu-water nanofluid with a two-phase mixture model. Their investigations show that the multi-phase model is more accurate than the single phase model. Maiga *et al.* [3] studied numerically the turbulent flow and heat transfer behaviour of Al_2O_3-water nanofluid at various nanoparticle volume concentrations in a circular tube. In this study, $Re = 10^4$ to 5×10^5 and the fluid inlet temperature of 293.15 K were considered. Also, the effect of nanoparticle volume fraction and Reynolds number were presented and a new correlation was proposed. Their numerical outcomes revealed that the inclusion of nanoparticles into the base fluid enhanced the heat transfer rate with the increase of nanoparticle volume fraction. Similar investigation was carried out by Bianco *et al.* [4] using both single-phase and multi-phase approaches and it was also found that the accuracy of the multi-phase mixture model is better than the single-phase model.

Namburu *et al.* [5] analysed numerically the forced convective flow and heat transfer behaviour of EG-water based CuO, Al_2O_3 and SiO_2 nanofluids flow through a circular tube. It is shown that nanofluids have higher viscosity, thermal conductivity and heat transfer rate compared to the base fluid. Akbari *et al.* [6] carried out a numerical investigation on the

turbulent forced convection flow in a horizontal tube. It is observed that the thermal predictions by two-phase model are very sensitive to the particle volume concentration, and the single-phase and two-phase models predict almost identical hydrodynamic fields. Kumar [7] studied numerically the heat transfer behaviour of Al_2O_3-water nanofluid using the single phase approach covering both laminar and turbulent flow regime. In this study, $Re = 10 \times 10^3$ to 30×10^3 and the fluid inlet temperature 315 K are considered. It is found that heat transfer rate significantly enhanced in the turbulent flow regime compared to that in the laminar flow regime.

Most recently, Saha and Paul [1] have examined the effect of volume concentration, diameter and Brownian motion of nanoparticles on the convective heat transfer of Al_2O_3 and TiO_2-water nanofluids using a single-phase numerical model. The aim of this piece of work is to extend the numerical model to investigate the effects of multi-phase flow of Al_2O_3 and TiO_2-water nanofluids. Particular attention is paid to the entropy generation of these two nanofluids and importantly, how the performance factor of nanofluids is varied if the numerical simulation is switched from the single- to multi-phase model.

2. Mathematical modelling

Eulerian-Eulerian mixture model is used to model the multi-phase flows with the assumption that the phases between fluid and solid particles move at a same velocity with a very strong coupling between them. Also, the phases are supposed to be interpenetrating, that means each phase has its own velocity vector field and within any control volume there is a volume concentration of each phase. It should also be noted that the mixture model solves the continuity, momentum and energy equations for the mixture and the volume fraction equation for the secondary phases. An axi-symmetric model is considered to describe the characteristics of nanofluids flowing through a straight circular pipe under a constant heat flux boundary condition and within a turbulent flow regime. It consists of a pipe with length L of 1.0 m and a circular section with diameter, D_h of 0.019 m as shown in Figure 1. The flow and thermal fields are assumed to be axisymmetric with respect to the horizontal plane parallel to the *x*-axis.

3. Governing equations

The dimensional steady-state governing equations of fluid flow and heat transfer for the two-phase mixture model have been presented and the following assumptions are made:

i. Fluid flow is incompressible, Newtonian and turbulent,

ii. The Boussinesq approximation is negligible as the pipe is placed horizontally,

iii. Nanoparticles are spherical and uniform in size and shape,

iv. The compression work and the viscous dissipation are negligible.

Under the above assumptions, the governing equations for the mixture model can be expressed as [8]:

Continuity equation:

$$\nabla.\left(\rho_m \vec{V}_m\right) = 0 \tag{1}$$

Momentum equation:

$$\nabla.\left(\rho_m \vec{V}_m \vec{V}_m\right) = -\nabla P_m + \nabla.\left[\mu_m \nabla \vec{V}_m - \sum_{s=1}^{n} \chi_s \rho_s \overline{v_s}\ \overline{v_s}\right] + \nabla.\left(\sum_{s=1}^{n} \chi_s \rho_s \vec{V}_{dr,s}\ \vec{V}_{dr,s}\right) \tag{2}$$

Energy equation:

$$\nabla.\left[\sum_{s=1}^{n} \chi_s \vec{V}_s (\rho_s H_s + P_m)\right] = \nabla.\left(\lambda_m \nabla T - C_p\ \rho_m \overline{vt}\right) \tag{3}$$

Volume fraction equation:

$$\nabla.\left(\chi_p\ \rho_p \vec{V}_m\right) = -\nabla.\left(\chi_p\ \rho_p \vec{V}_{dr,p}\right) \tag{4}$$

where $\vec{V}_m$, ρ_m, μ_m and λ_m are the mass-average velocity, mixture density, viscosity of the mixture and mixture thermal conductivity coefficient respectively and defined as

$$\vec{V}_m = \sum_{s=1}^{n} \frac{\chi_s \rho_s \vec{V}_s}{\rho_m} \tag{5}$$

$$\rho_m = \sum_{s=1}^{n} \chi_s\ \rho_s \tag{6}$$

$$\mu_m = \sum_{s=1}^{n} \chi_s\, \mu_s \tag{7}$$

$$\lambda_m = \sum_{s=1}^{n} \chi_s\, \lambda_s \tag{8}$$

where *n* is the number of phases, χ_s is the volume fraction of phase *s* and H_s is the sensible enthalpy for phase *s*. The drift velocity ($\vec{V}_{dr,s}$) for the secondary phase *s* which is defined as

$$\vec{V}_{dr,s} = \vec{V}_s - \vec{V}_m. \tag{9}$$

The relative or slip velocity is defined as the velocity of the secondary phase (*s*) relative to the velocity of the primary phase (*f*):

$$\vec{V}_{sf} = \vec{V}_s - \vec{V}_f. \tag{10}$$

Then the drift velocity related to the relative velocity becomes

$$\vec{V}_{dr,s} = \vec{V}_{sf} - \sum_{s=1}^{n} \vec{V}_{fs} \frac{\chi_s \rho_s}{\rho_m}. \tag{11}$$

Manninen *et al.* [9] and Naumann [10] proposed the following respective equations for the calculation of the relative velocity, $\vec{V}_{pf}$, and the drag function, f_{drag}.

$$\vec{V}_{pf} = \frac{\rho_p d_p^2}{18\mu_f f_{drag}} \frac{\rho_p - \rho_m}{\rho_p} \vec{a} \tag{12}$$

$$f_{drag} = \begin{cases} 1 + 0.15 Re_p^{0.687} & Re_p \leq 1000 \\ 0.0183 Re_p & Re_p > 1000 \end{cases} \tag{13}$$

where the acceleration $\vec{a}$ is determined by

$$\vec{a} = -\left(\vec{V}_m . \nabla\right) \vec{V}_m \,, \tag{14}$$

and d_p is the diameter of the nanoparticles of secondary phase *s* and $\vec{a}$ is the secondary phase particle's acceleration, *T* is the temperature, *P* is the pressure.

4. Turbulence modelling

Realizable $\kappa - \epsilon$ turbulence model of Shih *et al.* [11] is used in the multi-phase model, and a detailed investigation was carried out in Saha and Paul [1] to assess its suitability in the turbulent nanofluid simulations. The equations for the turbulent kinetic energy (κ) and dissipation rate of turbulent kinetic energy (ϵ) used in the realizable multi-phase $\kappa - \epsilon$ turbulent model are given by:

$$div(\rho_m V_m \kappa) = div\left\{\left(\mu_m + \frac{\mu_{t,m}}{\sigma_k}\right) grad\ \kappa\right\} + G_{\kappa,m} - \rho_m \epsilon \tag{15}$$

and

$$div(\rho_m V_m \epsilon) = div\left\{\left(\mu_m + \frac{\mu_{t,m}}{\sigma_\epsilon}\right) grad\ \epsilon\right\} + \rho_m C_1 S - \rho_m C_2 \frac{\epsilon^2}{\kappa + \sqrt{\nu\epsilon}} \tag{16}$$

where

$$C_1 = max\left[0.43, \frac{\eta}{\eta + 5}\right], \eta = S\frac{\kappa}{\epsilon} \text{ and } S = \sqrt{2\, S_{ij}\, S_{ij}} \tag{17}$$

In these equations, G_κ represents the generation of turbulence kinetic energy due to the mean velocity gradients, determined from $\mu_{t,m} S^2$ where, *S* is the modulus of the mean rate-of-strain tensor, σ_k and σ_ϵ are the effective Prandtl numbers for turbulent kinetic energy and rate of dissipation, respectively; and μ_t is modelled as

$$\mu_{t,m} = \frac{\rho_m \kappa^2}{\epsilon}\left(A_0 + A_s \frac{\kappa U^*}{\epsilon}\right)^{-1} \tag{18}$$

where A_0 and A_s are the model constants given as $A_0 = 4.04$ and $A_s = \sqrt{6cos\phi}$ respectively with $\phi = \left(3cos^{-1}\sqrt{6W}\right)^{-1}$ and the formulations for U^* and W depend on the angular velocity. In Eqs. (15) and (16); the model constants are $C_2 = 1.9,\ \sigma_k = 1.0$ and $\sigma_\epsilon = 1.2$ [8].

5. Entropy generation

The total entropy generation equation for a circular pipe of length *L* is proposed by Ratts and Raut [12] and defined as

$$E_{gen} = E_{gen,Th} + E_{gen,fl} \tag{19}$$

where the first term on the right hand side of Eq. (19) is the thermal entropy generation and the second term is the frictional entropy generation. These two terms are defined respectively as

$$E_{gen,Th} = \frac{\pi D_h^2\, L\, \dot{q}_s^2}{\lambda_{nf}\, \overline{Nu}\, T_{avg}} \tag{20}$$

$$E_{gen,fl} = \frac{32\dot{m}^3 f L}{\rho_{nf}^2 \pi^2 D_h^5\, T_{avg}} \tag{21}$$

where T_{avg} is the average temperature defined as follows:

$$T_{avg} = \frac{(T_{in} - T_{out})}{ln\left(\frac{T_{in}}{T_{out}}\right)} \tag{22}$$

6. Boundary conditions

To solve the set of non-linear governing equations presented above, appropriate boundary conditions are necessary and thus considered in the numerical simulations and have already described in Saha and Paul [1]. However, in the multi-phase mixture model, the boundary conditions used in the single-phase model are specified for both the fluid and solid phases as well as for the mixture. Also, for the solid phase, nanoparticle volume fraction is used and further details about the boundary conditions of the mixture model are given in [8].

7. Nanofluids physical properties

Thermophysical properties of density and heat capacitance of the nanofluid are calculated by using the formulas which are considered as classical relationships between the base fluid and nanoparticles, proposed by Buongiorno [13]. Also, because of the lack of experimental results and correlations, which depend on the nanoparticle size diameter as well as

temperature in relation to the thermophysical properties of nanofluid, the correlations proposed by Corcione [14] for the thermal conductivity and dynamic viscosity are used in our analysis. The density, specific heat capacity, kinematic viscosity and thermal conductivity of water as well as Al_2O_3 and TiO_2 were calculated by the correlations proposed by Kays and Crawford [15], Masuda *et al.* [16], Powel *et al.* [17] and Smith *et al.* [18]. The details are given in Saha and Paul [1].

8. Numerical methods and grid sensitivity analysis

Computational domain is formed by using the commercial pre-processor software GAMBIT which is also used for meshing and setting up the boundary conditions. Then the governing equations for the continuity, momentum, energy and other scalars such as turbulence together with the suitable boundary conditions are discretised and hence solved by using the Finite volume solver Fluent 6.3.26. Further details are given in Saha and Paul [1]. Moreover, in order to ensure the accuracy as well as the consistency of the numerical results, extensive computations have been performed to identify the number of grid points that produce a suitable arrangement result which will be applicable to determine the flow and thermal field inside the pipe. The grid sensitivity study is performed and the details are also given in Saha and Paul [1].

9. Validation of the numerical results

Accuracy of the numerical results for the base fluid (water) against existing correlations for the different Reynolds number, *Re* = 10×10^3 to 100×10^3, has been tested in Saha and Paul [1]. In Figure 2, a comparison between the present result and that of Pak and Cho [19] is shown graphically for the Al_2O_3-H_2O nanofluid and $\chi = 0.01, 0.04$ and 0.06. It is shown that the present numerical results are in very strong agreement with the correlation of Pak and Cho [19] which is completely empirical as referred by Buongiorno [13]. The details of the Pak and Choi [19] correlation, the dynamic viscosity and the thermal conductivity model used in this analysis are also given in Saha and Paul [1].

10. Results and discussion

Numerical simulations are carried out using Al_2O_3-H_2O and TiO_2-H_2O nanofluids, with the following range of governing parameters: Reynolds number from $Re = 10 \times 10^3$ to 100×10^3, Prandtl number from 7.04 to 20.29, particle volume concentration of 4% and 6%, and diameter of nanoparticles of $10, 20, 30$ and $40\ nm$. The results and discussion presented hereafter focusing on the effects of particle volume concentration, mean diameter and

Brownian motion of different nanoparticles and different Reynolds number on the flow and heat transfer performance as well as on the entropy generation of the nanofluids in the turbulent flow regime.

10.1 Nanoparticles volume concentration

Figure 3 shows the radial variation of the nanoparticles volume concentration at the outlet for the Al_2O_3-water nanofluid with $Re = 100 \times 10^3$ and d_p = 10 *nm*. It is found that the nanoparticle volume concentration is absolutely uniform and constant, which further indicates that the nanoparticle distribution in the fluid is also uniform. This is valid in a sense that the suspended nanoparticles remain uniform in the fluid – an assumption that is implicitly integrated in the single-phase model. The similar behavior is also observed for all the Reynolds numbers with different diameter size of nanoparticles using both the Al_2O_3-water and TiO_2-water nanofluids. This again provides strong evidence that the above assumption is completely realistic for all the flow Reynolds numbers undertaken even though the drift velocity equation was valid for the μm and *mm* size particles. It is also to be noted that the similar behaviour was found by other researchers (Behzadmehr *et al.* [2], Bianco *et al.* [4]).

10.2 Average shear stress coefficient ratio

Figure 4 shows the effect of various volume concentrations, different nanoparticle size diameters of Al_2O_3-water and TiO_2-water nanofluids on the average shear stress ratio defined as the ratio of the average shear stresses, $\bar{\tau}_\tau = \overline{\tau_{nf}}/\bar{\tau}_f$. From the investigation, it is found that the average shear stress ratio has increased with an increase in the nanoparticle volume concentration and decrease in the nanoparticle size diameter from 40 to 10 *nm* and such enhancement is independent to the Reynolds number. For example, when the Reynolds number and particle volume concentration for the Al_2O_3-water nanofluid are fixed to *Re* = 20×10^3 and $\chi = 4\%$, the average shear stresses ($\bar{\tau}_\tau$) has a value of 1.99, 2.19, 2.54 and 3.58 for d_p = 40, 30, 20 and 10 *nm* respectively. For a higher particle volume concentration, e.g. $\chi = 6\%$, $\bar{\tau}_\tau$ increases again and has a value of 3.36, 4.06, 5.69 and 14.35 for d_p = 40, 30, 20 and 10 *nm* respectively. Similar behaviors have also been observed for the TiO_2-water nanofluid and therefore, it can be generally concluded that the increase of the average shear stress ratio with respect to the nanoparticle volume concentration as well as the nanoparticle size diameter emerges to be noticeably more significant for both the Al_2O_3-water and TiO_2-

water nanofluids. Such enhancement of the average shear stress ratio may be due to the adverse effects of increase frictional force or pressure in the nanofluids.

10.3 Heat transfer performance

Figure 5 shows the results of the effect of various volume concentrations, nanoparticle size diameter of Al_2O_3-water and TiO_2-water nanofluids on the average Nusselt number. A comparison of the findings with those of the base fluid (water) is also made. It is shown in this figure that the average Nusselt number increases with the increase of Reynolds number and particle volume concentration when the nanoparticle size diameter changes from 40 *nm* to 10 *nm*. Also it can be clearly seen that the average Nusselt number of the nanofluids is higher than that of the base fluid water at any given Reynolds number. The explanation for such enhancement in the average Nusselt number is associated to different aspects such as enhancement of thermal conductivity, nanoparticle size and shapes, Brownian motion of particles, decrease in boundary layer thickness and delay in boundary layer growth.

However, the average Nusselt number is very sensitive to the nanoparticle types and diameter, and in general the heat transfer rate increases as the nanoparticle size diameter decreases. For example, for the Al_2O_3–water nanofluid and χ = 4% and 6% with d_p = 10 *nm*, the maximum enhancement is approximately 23.26% and 62.34% respectively, while for d_p = 20 *nm*, it is approximately 15.87% and 35.76% respectively. However, for the TiO_2–water nanofluid and χ = 4% and 6% with d_p = 10 *nm*, the maximum enhancement is approximately 23.60% and 62.53% respectively, while for d_p = 20 *nm*, it is approximately 16.31% and 36.12% respectively. Similar trend is observed as the nanoparticle size diameter increases from 20 to 30 *nm* or 30 to 40 *nm*. In order to get a higher heat transfer rate, the 10 *nm* particle diameter is found to be best for both the Al_2O_3–water and TiO_2–water nanofluids. This result has a close link to the corresponding flow velocity such that the heat transfer enhancement becomes more significant when the Reynolds number is increased. Further to note that the TiO_2–water nanofluid gives the higher heat transfer enhancement than Al_2O_3–water irrespective to the change in Reynolds number, nanoparticle volume concentration and diameter, although its thermal conductivity is lower than that of Al_2O_3–water nanofluid. For a quantitative assessment, values of the minimum and maximum increment in the Nusselt number of different nanofluids are shown in Table 1 for different nanoparticle volume concentration and size diameter. Smaller diameter and Brownian motion of nanoparticles assist to increase the viscosity for the same particle volume concentration, hence making an

impact on the Nusselt number enhancement. This is reasonable because smaller nanoparticles with higher velocity move faster than the large particles thus reduce the possibility of collision with each other. Also, nanoparticles with smaller diameter are more in number compared to large nanoparticles and therefore make a strong contact with the neighbouring fluid over a greater surface area. Consequently, the process helps to increase the viscosity and thermal conductivity of nanofluids with a result in the heat transfer enhancement.

Table 1: Minimum and maximum increment (%) of the average Nusselt number for different nanofluids

	Al_2O_3-water				TiO_2-water			
d_p (nm)	χ = 4%		χ = 6%		χ = 4%		χ = 6%	
	min	max	min	max	min	max	min	max
10	18.58	23.26	58.60	62.34	21.07	23.60	60.25	62.53
20	11.44	15.87	30.83	35.76	14.61	16.31	33.53	36.12
30	07.81	12.53	21.25	27.30	11.09	12.95	25.42	27.72
40	06.43	10.84	16.47	22.65	09.92	11.28	21.31	23.09

10.4 Thermal performance factor

Thermal performance factor which is defined by the following equation (Suresh *et al*. [20]) is reported in Figure 6 for the different values of volume concentrations and nanoparticle size diameters.

$$\xi = \left(\frac{\overline{Nu}_{nf}}{\overline{Nu}_f}\right)\left(\frac{f_{nf}}{f_f}\right)^{\frac{1}{3}} \tag{23}$$

It is found that the thermal performance factor remains greater than one for all the possible cases considered and it is very close to the ratio of the average Nusselt number of nanofluid to the base fluid. Also the ratio of the friction factor of nanofluids to the base fluid is approximately close to 1. Hence it is possible to make a conclusion that the heat transfer enhancement is possible with little or without penalty in the pumping power. This may lead to less energy cost and more efficient for practical application. It is also clear that the thermal performance factor increases as the nanoparticle volume concentration increases and generally, a higher value of ξ is achieved for the small nanoparticle size diameter. This might be explained by the fact that the dynamic viscosity as well as the thermal conductivity of nanofluids increases with the particle volume concentration, hence the higher viscosity

reduces the boundary layer thickness resulting in the heat transfer enhancement whereas the higher thermal conductivity directs to an enhancement in the thermal performance factor.

10.5 Entropy generation analysis

Figure 7 shows the variation of the total entropy generation on the Al_2O_3-water and TiO_2-water nanofluids with the Reynolds number, volume concentrations nanoparticle size diameters. For $\chi = 4\%$ and Al_2O_3-water nanofluid, it is found that the total entropy generation decreases as the Reynolds number increases with the decrease of the nanoparticles size diameter. The main reason behind this fact is the decrease of the thermal entropy generation with the decrease of the nanoparticles size diameter. This happens because when the nanoparticle size diameter decrease from 40 to 10 *nm*, the heat transfer enhances significantly. It is also observed that the frictional entropy generation has insignificant effect on the reduction of the total entropy generation because the maximum value of the frictional entropy generation for all the Reynolds numbers and nanoparticles size diameter is always remained less than 1. It is further seen that the frictional entropy generation monotonically increases with the Reynolds number but decreases with the nanoparticles size diameter. This is due to the increase of the flow velocity. For $\chi = 6\%$ and Al_2O_3-water nanofluid, similar behaviour is observed for the entire nanoparticles size diameter except for d_p = 10 *nm*. It is found that for $\chi = 6\%$, d_p = 10 *nm* and $Re > 50 \times 10^3$, the velocity increases significantly and hence the frictional entropy generation becomes stronger. The optimal Reynolds number is found to be $Re = 60 \times 10^3$ for $\chi = 6\%$ and d_p = 10 *nm*, which minimises the total entropy generation. Again, for $Re > 60 \times 10^3$, the frictional entropy generation becomes more and more stronger and hence the total entropy generation started to rise. It is to be noted that the similar performance is also observed for the TiO_2-water nanofluid with the variation of the Reynolds number, nanoparticles volume concentration and nanoparticles size diameter. From this investigation, it is found that the Al_2O_3-water nanofluid shows higher total entropy generation than the TiO_2-water nanofluid. Values of the minimum and maximum thermal entropy generation of different nanofluids are shown in Table 2 for the different nanoparticles volume concentration and size diameter.

Table 2: Minimum and maximum values of the thermal entropy generation

	Al_2O_3-water				TiO_2-water			
d_p (nm)	χ = 4%		χ = 6%		χ = 4%		χ = 6%	
	min	max	min	max	min	max	min	max
10	8.65	59.01	6.32	42.70	8.67	59.31	6.37	43.13
20	9.51	64.50	7.86	53.42	9.52	64.53	7.90	53.54
30	9.94	67.12	8.55	57.73	9.95	67.22	8.58	58.09
40	10.20	68.78	8.99	60.96	10.21	68.89	9.01	60.98

10.6 Heat transfer enhancement analysis

Figure 8 shows the variation of the maximum heat transfer enhancement with the nanoparticle size diameters obtained by the single- (SPM) and multi-phase (MPM) models for the Al_2O_3-water and TiO_2-water nanofluids. It is found that the lower heat transfer rate is achieved using the single-phase model compared to that by the multi-phase model due to the fact that the assumption of fluid phase and nanoparticle phase are in thermal equilibrium and no-slip between them when using the single-phase model. It is to be noted that the interaction between the fluid and nanoparticles may not be negligible because of the slip velocity which may not be zero; therefore it is realistic to achieve the higher heat transfer rate using the multi-phase model.

10.7 Performance evaluation criterion

Performance evaluation criterion (PEC) is defined as follows (Roy *et al*.[21]):

$$PEC = \frac{\rho_{nf}\, Cp_{nf}\, \Delta T}{\Delta p} \tag{24}$$

where ΔT and Δp are respectively the temperature and pressure differences between the outlet and inlet of the pipe. Figure 9 shows the variation of the performance evaluation criterion (PEC) values and it is shown that they decrease as the Reynolds number increases with the increase of the nanoparticles size diameter. For $\chi = 6\%$ and the Al_2O_3-water nanofluid, similar behaviour is observed for the entire nanoparticle size diameter and this is also true for the TiO_2-water nanofluid. However, the TiO_2-water nanofluid shows a slightly higher performance evaluation criterion than the Al_2O_3-water nanofluid and therefore, it is concluded that the TiO_2-water nanofluid is the most energy efficient coolant for this particular system.

10.8 Correlations

From the numerical results and using the non-linear regression analysis, the following correlations are proposed for the calculation of the average Nusselt number with the Reynolds number, Prandtl number and nanoparticle size diameter. These correlations are valid when the Brownian motion of nanoparticles is taken into account. Also, the values of maximum standard deviation of error are reported to be 4.81% and 3.77% for the Al_2O_3 and TiO_2 nanofluids respectively. Further, comparisons between the numerical results of the average Nusselt number and computed by the proposed correlations are presented in Fig. 10. This figure shows a good agreement between the numerical results and the proposed correlations.

Al_2O_3-H_2O nanofluid : $$\overline{Nu} = 0.01260\, Re^{0.85589} Pr^{0.44709} \left(\frac{d_f}{d_p}\right)^{-0.00176} \quad (25)$$

TiO_2-H_2O nanofluid : $$\overline{Nu} = 0.01518\, Re^{0.84071} Pr^{0.44083} \left(\frac{d_f}{d_p}\right)^{-0.00534} \quad (26)$$

where

$10 \times 10^3 \leq Re \leq 100 \times 10^3,\ 8.45 \leq Pr \leq 20.29,\ 10 \leq d_p(nm) \leq 40,\ 2 \leq \chi(\%) \leq 6.$

11. Conclusion

Numerical simulations have been carried out on the turbulent mixed convection heat transfer of the Al_2O_3-water and TiO_2-water nanofluids flowing through a horizontal circular pipe using the two-phase mixture model. The effects of Reynolds and Prandtl numbers, two different nanofluids, nanoparticle volume concentration, Brownian motion and diameter size of nanoparticles on the flow and heat transfer have been investigated. According to our findings, the following conclusion are made and summarised as follows:

(a) It was found that for χ = 4% and 6%, the Al_2O_3-water and TiO_2-water nanofluids, with the 10 to 40 *nm* particle size diameters and Brownian motion of nanoparticles, the average Nusselt number is significantly higher than the base fluid (water). It was also seen that the average shear stress ratio becomes superior for small diameter of nanoparticles compared to the large diameter of nanoparticles with the increase of the nanoparticle volume concentration.

(b) The Darcy friction factor of nanofluids has no significant effect compared to the base fluid (water) and hence induces no extra penalty in the pump power.

(c) The nanofluid with 10 *nm* and χ = 6% shows the higher thermal performance factor for any Reynolds numbers and nanoparticles size diameter.

(d) The TiO_2–water nanofluid gives the higher heat transfer enhancement than the Al_2O_3–water nanofluid for all the Reynolds numbers, nanoparticle volume concentration as well as nanoparticles size diameter.

(e) The Al_2O_3-water nanofluid shows the higher total entropy generation than the TiO_2-water nanofluid. But, the TiO_2-water nanofluid shows slightly higher performance evaluation criterion values than the Al_2O_3-water nanofluid.

Furthermore, we have found that the TiO_2-H_2O nanofluid shows better heat transfer performance than that of the Al_2O_3-H_2O nanofluid using the multi-phase model compared with the results of the single-phase model. Since TiO_2 nanoparticles are more environment-friendly and eco-friendly [22] than the Al_2O_3 nanoparticles, it is better to use the TiO_2-water nanofluid in any practical engineering applications.

Nomenclature

a	Acceleration (m/s^2)
A_0, A_1, C_1, C_2, C_μ	Model constant
C_p	Specific heat capacity (J/kg K)
D	Einstein diffusion coefficient
D_h	Diameter of a pipe (m)
d_f	Fluid molecular diameter (m)
d_p	Diameter of nanoparticle (nm)
E_{gen}	Entropy generation (W/K)
f	Darcy friction factor
f_{drag}	Drag function
f_μ	Dumping function
G_k	Generation of turbulent kinetic energy
H	Enthalpy (J/kg)
I	Turbulent intensity
L	Length (m)
M	Molecular weight of the base fluid
$\dot{m}$	Mass flow rate (kg/s)
N	Avogadro number
N_x, N_r	Number of grid distribution in axial and radial directions
Nu	Nusselt number
P	Pressure (N/m^2)
Pr	Prandtl number
$\dot{q}_s$	Heat flux of the pipe (W/m^2)
R	Radius of a pipe (m)
Re	Reynolds number
r	Radial coordinate (m)
S	Modulus of the mean rate of strain tensor
T, t	Time average and fluctuating temperature (K)
u_B	Nanoparticle particle mean Brownian velocity (m/s)
u_τ	Friction velocity (m/s)
V, v	Time average and fluctuating velocity components (m/s)
x	Axial coordinate (m)

Greek symbols

ρ	Density (kg/m^3)
μ	Dynamic viscosity (kg/ ms)
λ	Thermal conductivity (W/m K)
κ	Turbulent kinetic energy (m^2/s^2)
ϵ	Dissipation rate of Turbulent kinetic energy (m^2/s^3)
ν	Kinematic viscosity (m^2/s)
σ_t	Constant of turbulent Prandtl number
μ_t	Turbulent molecular viscosity
σ_κ	Effective Prandtl number for turbulent kinetic
σ_ϵ	Effective Prandtl number for rate of dissipation
χ	Nanoparticle volume concentration
ξ	Thermal performance factor
τ_D	Time (s)
$\overline{\tau}_\tau$	Ratio of average shear stresses

Subscripts

avg	Average
eff	Effective
f	Base fluid
fl	Frictional
fr	Freezing
in	Inlet
m	Mixture
mean	Mean
nf	Nanofluid
out	Outlet
p	Nanoparticle
s	Secondary phase
w	Wall
t	Turbulent
Th	Thermal

References

[1] G. Saha, M.C. Paul, Numerical analysis of heat transfer behaviour of water based Al_2O_3 and TiO_2 nanofluids in a circular pipe under the turbulent flow condition, International Communication in Heat and Mass Transfer, 56 (2014) 96-108.

[2] A. Behzadmehr, M. Saffar-Avval, N. Galanis, Prediction of turbulent forced convection of a nanofluid in a tube with uniform heat flux using a two phase approach, International Journal of Heat and Fluid Flow, 28 (2007) 211-219.

[3] S.E.B. Maiga, C.T. Nguyen, N. Galanis, G. Roy, T. Mare, M. Coqueux, Heat transfer enhancement in turbulent tube flow using Al_2O_3 nanoparticle suspension, International Journal of Numerical Methods for Heat and Fluid Flow, 16 (2006) 275-292.

[4] V. Bianco, O. Manca, S. Nardini, Numerical investigation on nanofluids turbulent convection heat transfer inside a circular tube, International Journal of Thermal Sciences 50 (2011) 341-349.

[5] P.K. Namburu, D.K. Das, K.M. Tanguturi, R.S. Vajjha, Numerical study of turbulent flow and heat transfer characteristics of nanofluids considering variable properties, International Journal of Thermal Sciences 48 (2009) 290–302.

[6] M. Akbari, N. Galanis, A. Behzadmehr, Comparative assessment of single and two-phase models for numerical studies of nanofluid turbulent forced convection International Journal of Heat and Fluid Flow, 37 (2012) 136-146.

[7] P. Kumar, A CFD study of heat transfer enhancement in pipe flow with Al_2O_3 nanofluid, World Academy of Science, Engineering and Technology, 81 (2011) 746-750.

[8] Fluent 6.3 user guide, Fluent Inc., Lebanon, 2006.

[9] M. Manninen, V. Taivassalo, S. Kallio, On the mixture model for multiphase flow, Technical research centre of Finland, 288 (1996) 9-18.

[10] L. Schiller, A. Naumann, A drag coefficient correlation, Z. Ver. Deutsch. Ing., 77 (1935) 318-320.

[11] T.H. Shih, W.W. Liou, A. Shabbir, Z. Yang, J. Zhu, A new k-ϵ eddy viscosity model for high Reynolds number turbulent flows, Computational Fluids, 24 (1995) 227-238.

[12] E.B. Ratts, A.G. Raut, Entropy generation minimization of fully developed internal flow with constant heat flux, Journal of Heat Transfer, 126 (2004) 656-659.

[13] J. Buongiorno, Convective transport in nanofluids, Journal of Heat Transfer, 128 (2006) 240-250.

[14] M. Corcione, Empirical correlating equations for predicting the effective thermal conductivity and dynamic viscosity of nanofluids, Energy Conversion and Management, 52 (2011) 789-793.

[15] W.M. Kays, M.E. Crawford, Convection heat and mass transfer, 2nd ed., McGraw Hill, New York, 1980.

[16] H. Masuda, A. Ebata, K. Teramae, N. Hishinuma, Alternation of thermal conductivity and viscosity of liquid by dispersing ultra-fine particles (dispersion of Al_2O_3, SiO_2 and TiO_2 ultra-fine particles), Netsu Bussei, 40 (1993) 227-233

[17] R.W. Powell, C.Y. Ho, P.E. Liley, Thermal conductivity of selected materials, United states department of commerce, National Bureau of standards, 1962.

[18] S.J. Smith, R. Stevens, S. Liu, G. Li, A. Navrotsky, J.B. Goates, B.F. Woodfield, Heat capacities and thermodynamic functions of TiO_2 anatase and rutile: analysis of phase stability, Am. Mineral, 94 (2009) 236-243.

[19] B.C. Pak, Y.I. Cho, Hydrodynamic and heat transfer study of dispersed fluids with submicron metallic oxide particles, Experimental Heat Transfer, 11 (1998) 151-170.

[20] S. Suresh, M. Chandrasekar, S.C. Sekhar, Experimental studies on heat transfer and friction factor characteristics of CuO/water nanofluid under turbulent flow in a helically dimpled tube, Experimental Thermal and Fluid Science 35 (2011) 542-549.

[21] G. Roy, L. Gherasim, F. Nadeau, G. Poitras, C.T. Nguyen, Heat transfer performance and hydrodynamic behavior of turbulent nanofluid radial flows, International Journal of Thermal Sciences, 58 (2012) 120-129.

[22] R. Mosurkal, L.A. Samuelson, K.D. Smith, P.R. Westmoreland, V.S. Parmar, F. Yan, Nanocomposites of TiO_2 and siloxane copolymers as environmentally safe flame retardant materials, Journal of Macromolecular Science Part A Pure and Applied Chemistry, 45 (2008) 924–946.

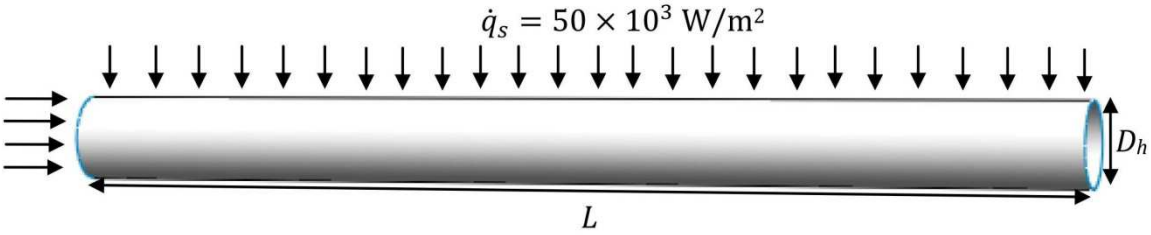

Figure 1: Schematic diagram of the geometry under consideration

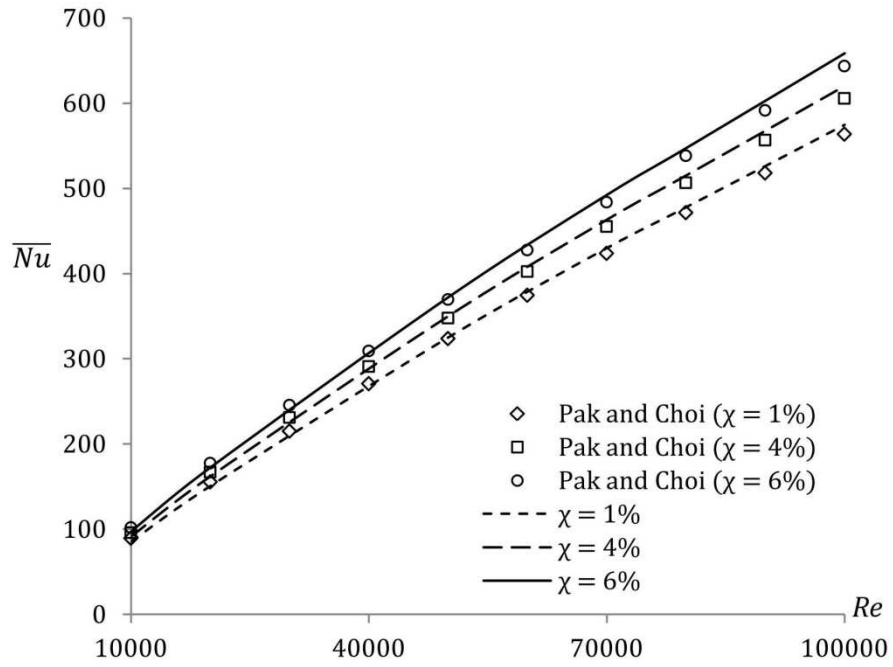

Figure 2: Comparison of the average Nusselt number for Al_2O_3-H_2O nanofluid with the Pak and Cho [19] correlation for different *Re*

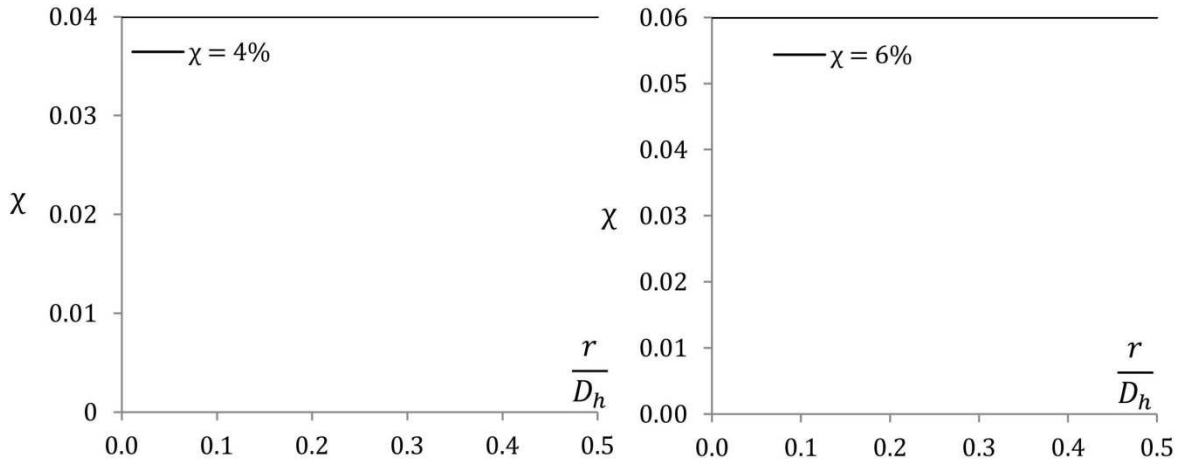

Figure 3: Variation of radial nanoparticles volume concentration at the outlet for Al_2O_3-water nanofluid with $Re = 100 \times 10^3$ and d_p = 10 *nm*

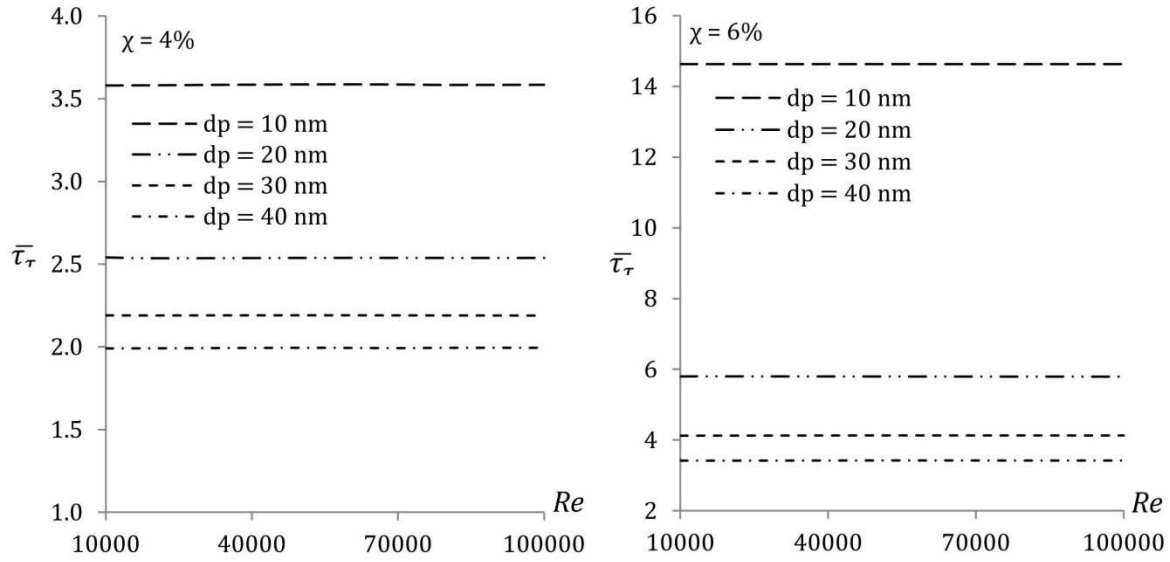

(a) Al_2O_3-H_2O nanofluid

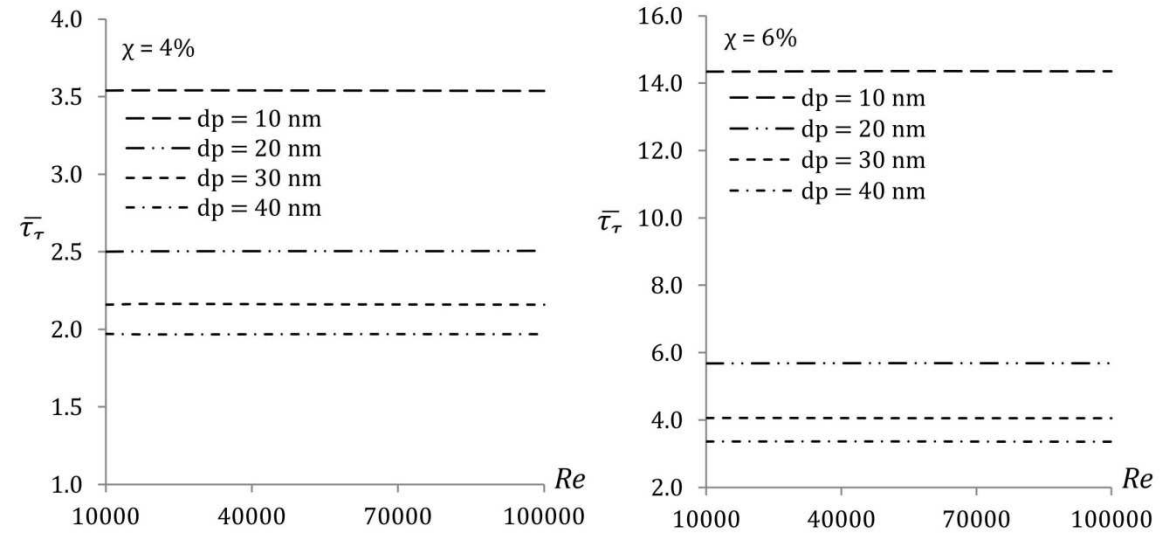

(b) TiO_2-H_2O nanofluid

Figure 4: Variation of average shear stress ratio with different Reynolds number for Al_2O_3-water and TiO_2-water nanofluids, nanoparticle volume concentration of 4% and 6% and nanoparticles size diameter of 10, 20, 30 and 40 *nm*

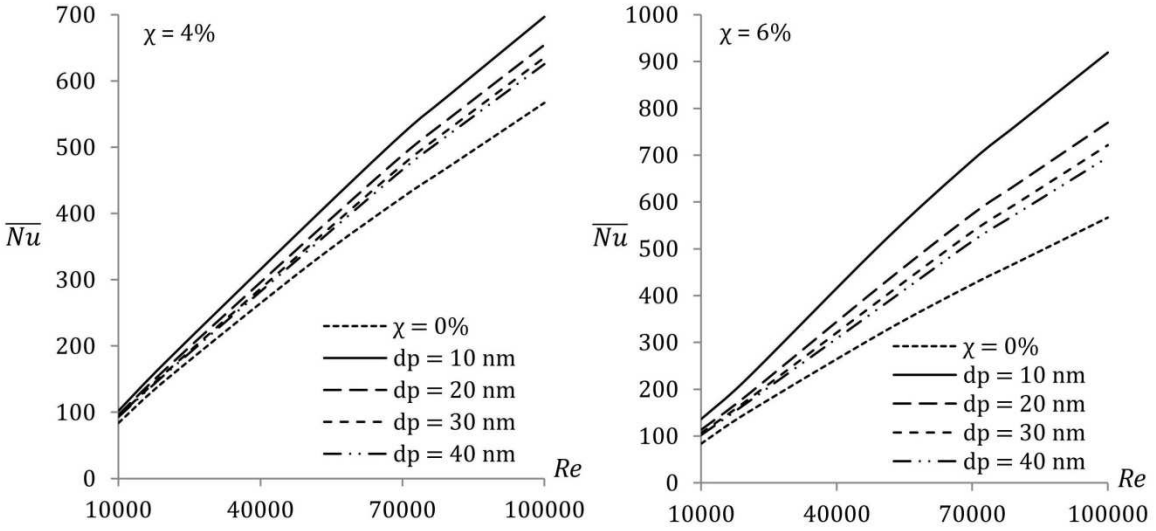

(a) Al_2O_3-H_2O nanofluid

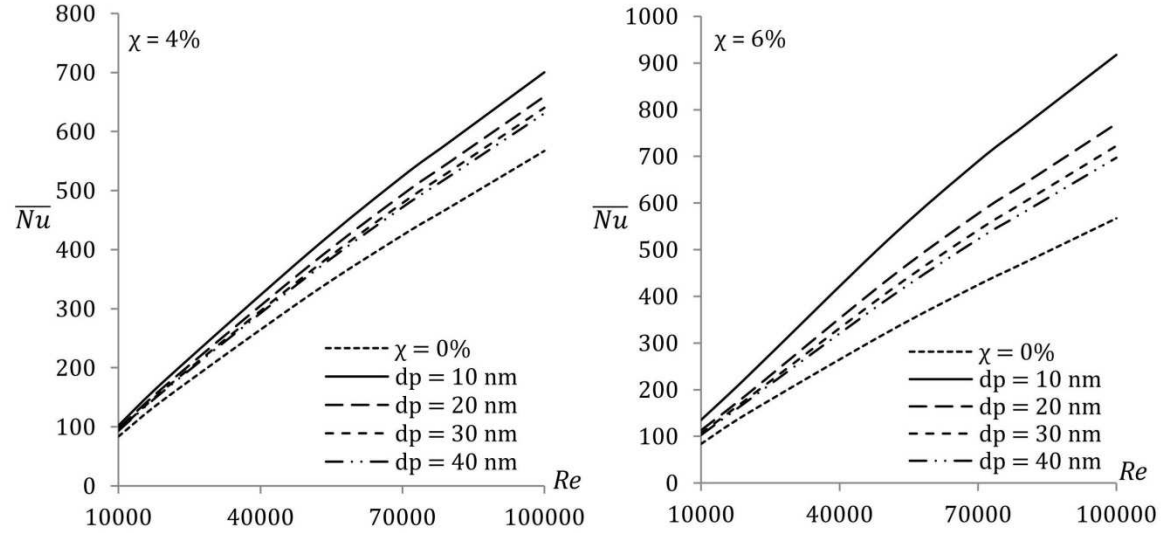

(b) TiO_2-H_2O nanofluid

Figure 5: Variation of average Nusselt number with different Reynolds number for Al_2O_3-water and TiO_2-water nanofluids, nanoparticles volume concentration of 4% and 6% and nanoparticles size diameter of 10, 20, 30 and 40 *nm*

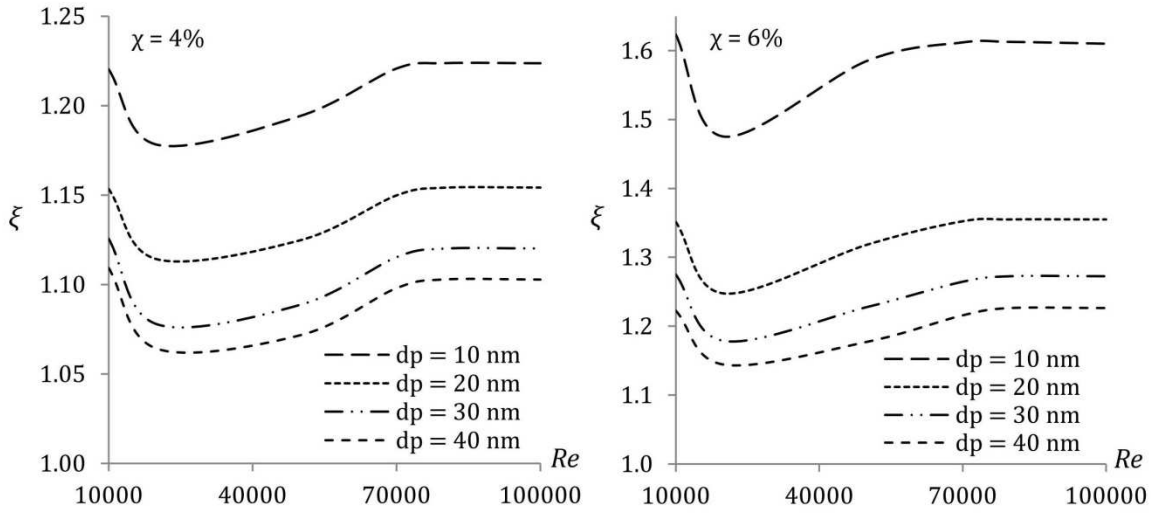

(a) Al_2O_3-H_2O nanofluid

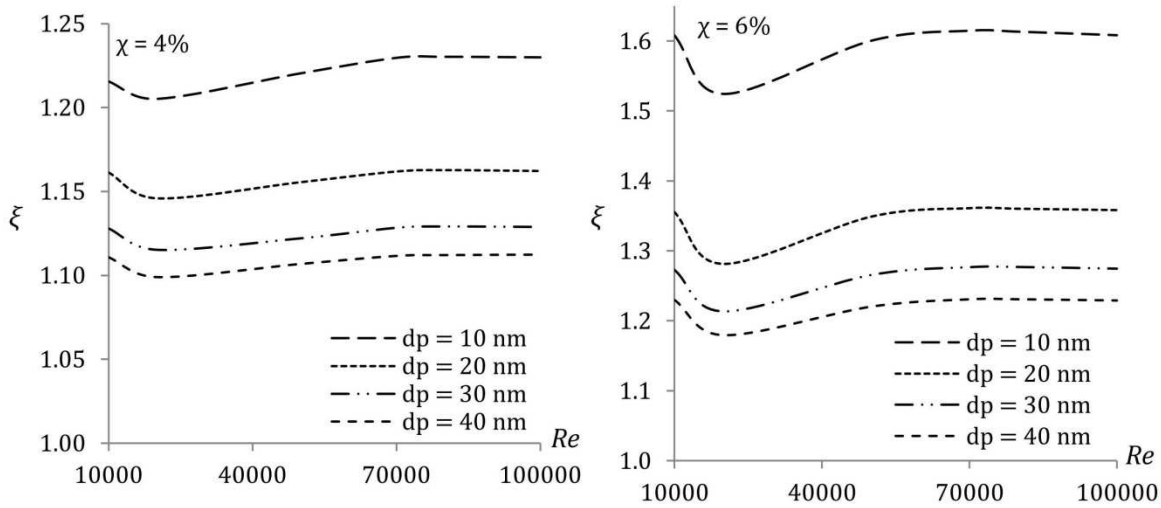

(b) TiO_2-H_2O nanofluid

Figure 6: Variation of thermal performance factor with different Reynolds number for Al_2O_3-water and TiO_2-water nanofluids, nanoparticles volume concentration of 4% and 6% and nanoparticles size diameter of 10, 20, 30 and 40 *nm*

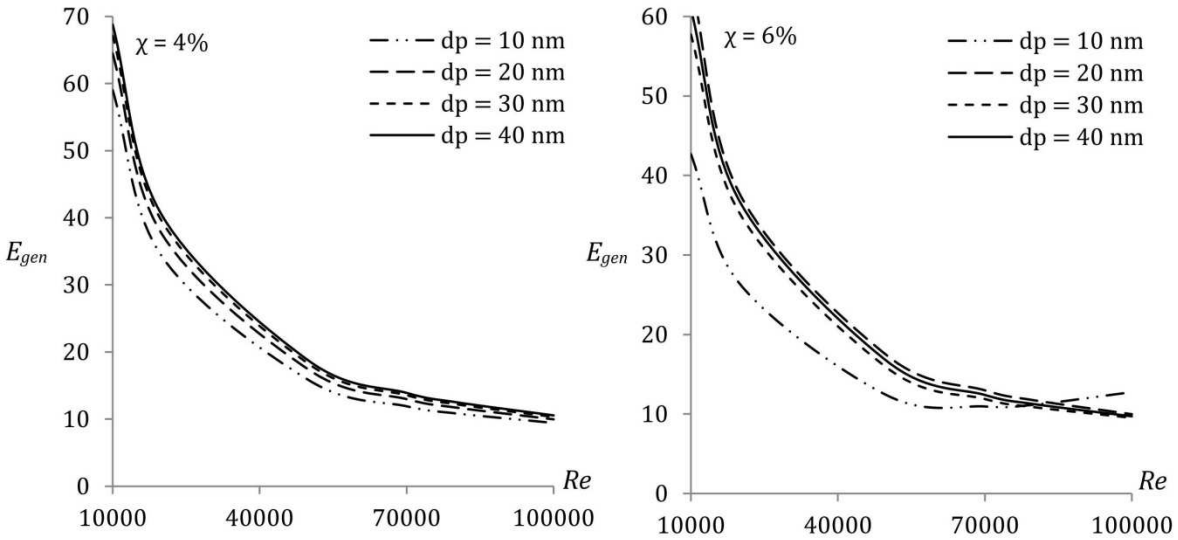

(a) Al_2O_3-H_2O nanofluid

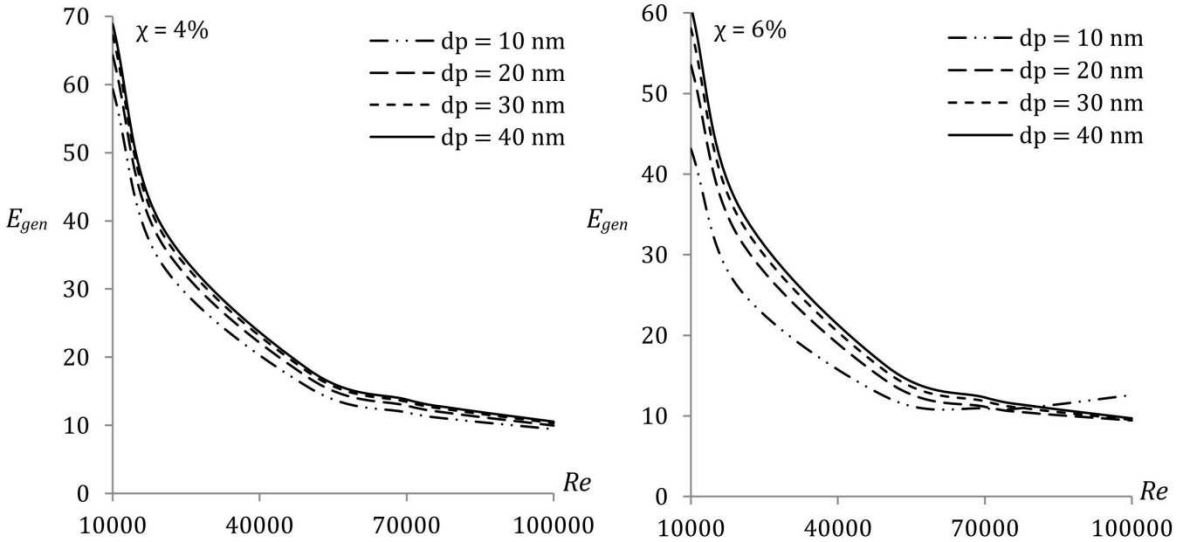

(b) TiO_2-H_2O nanofluid

Figure 7: Variation of total entropy generation with different Reynolds number for Al_2O_3-water and TiO_2-water nanofluids, nanoparticles volume concentration of 4% and 6% and nanoparticles size diameter of 10, 20, 30 and 40 *nm*

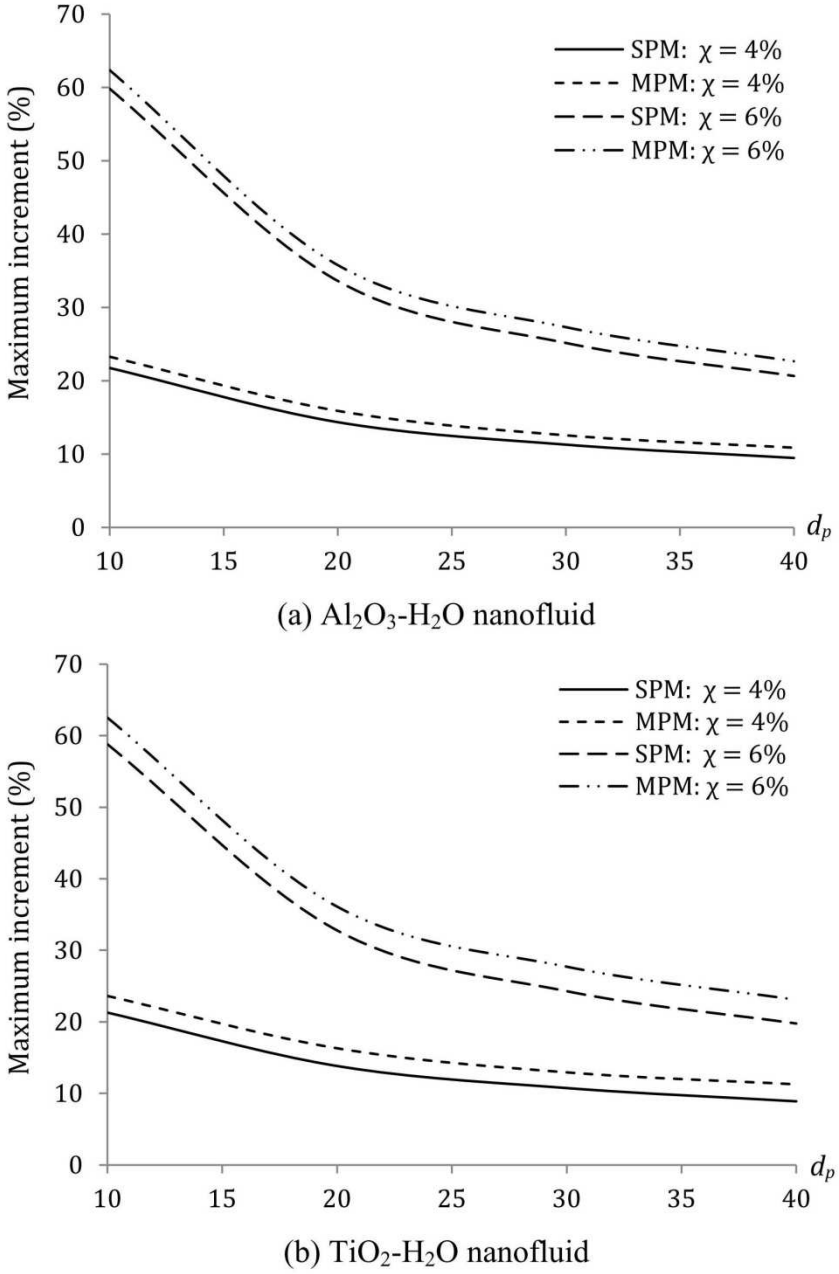

Figure 8: Variation of maximum heat transfer enhancement (%) with different nanoparticles size diameter for Al_2O_3-water and TiO_2-water nanofluids

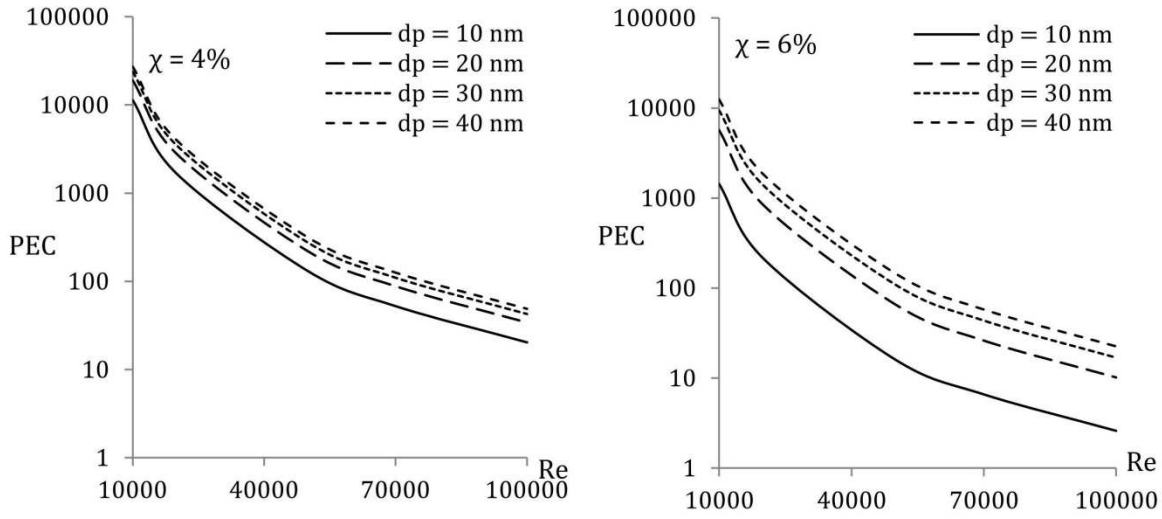

(a) Al_2O_3-H_2O nanofluid

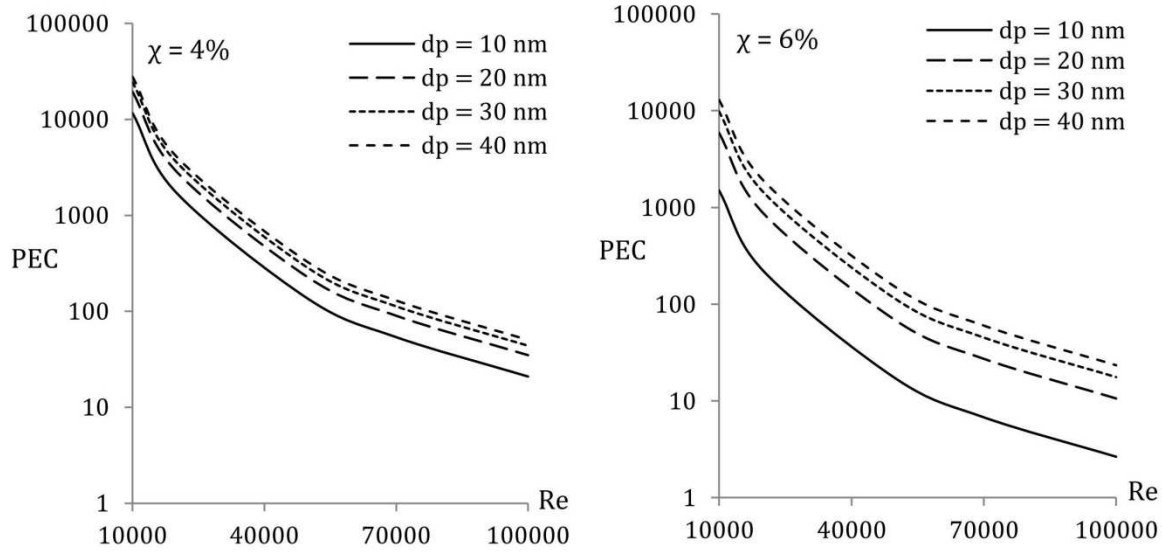

(b) TiO_2-H_2O nanofluid

Figure 9: Variation of performance evaluation criterion (PEC) with different nanoparticles size diameter for Al_2O_3-water and TiO_2-water nanofluids for different Reynolds number

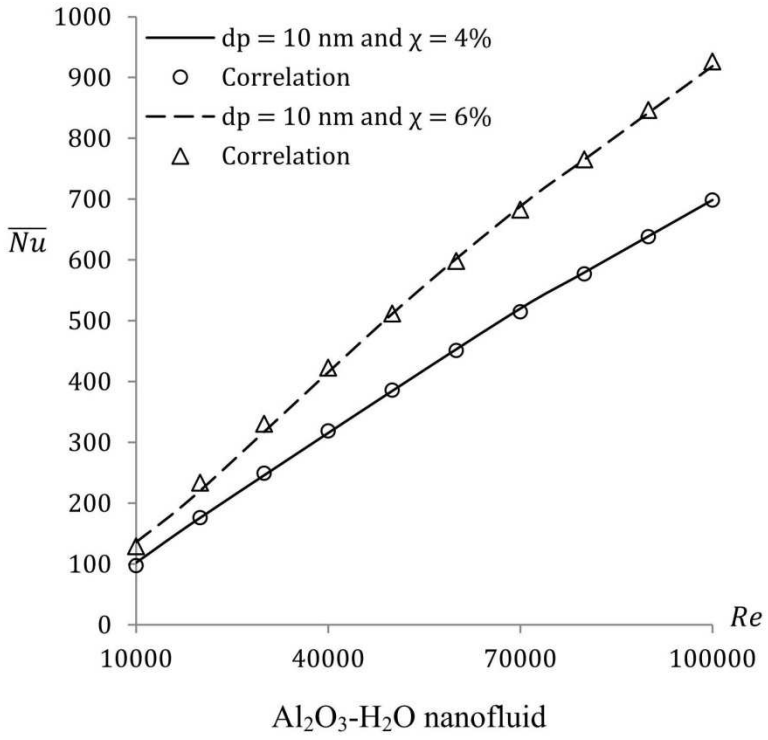

Al_2O_3-H_2O nanofluid

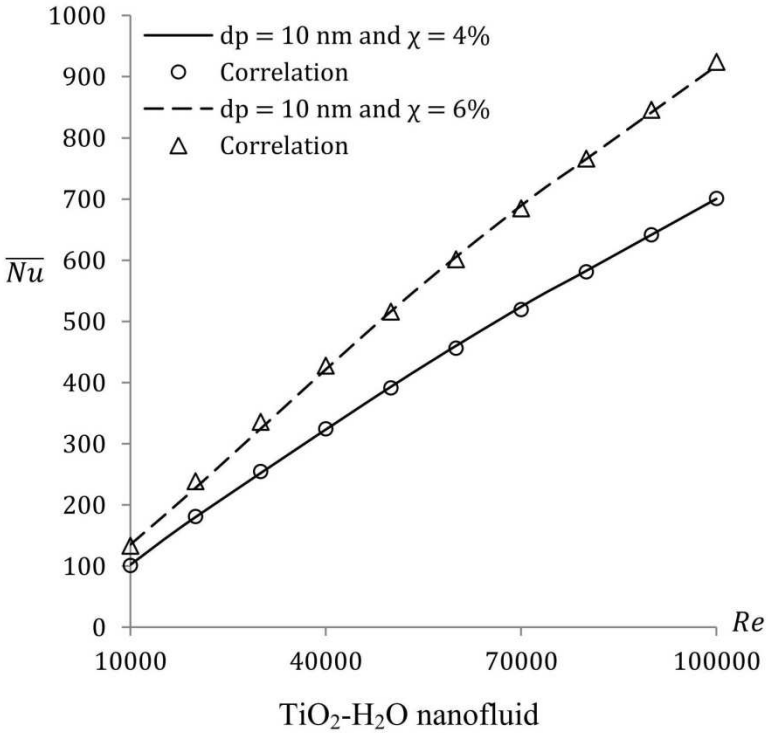

TiO_2-H_2O nanofluid

Figure 10: Comparisons of the proposed correlations with the numerical results for Al_2O_3-water and TiO_2-water nanofluids